

Top-Quark Decay Via the Anomalous Coupling $\bar{t}c\gamma$ at Hadron Colliders

T. Han^a, K. Whisnant^b, B.-L. Young^{b,c} and X. Zhang^b

^a*Department of Physics, University of California, Davis, CA 95616, USA*

^b*Department of Physics and Astronomy, Iowa State University, Ames, IA 50011, USA*

^c*Institute of Physics, Academia Sinica, Taipei, Taiwan*

Abstract

We determine the constraints on the anomalous top-quark coupling associated with the flavor-changing neutral current vertex $\bar{t}c\gamma$ from the limits on the b -quark rare decay $b \rightarrow s\gamma$ and non-standard top-quark decays. Based on these constraints, we discuss the experimental observability of the rare decay mode $t \rightarrow c\gamma$, both at the Fermilab Tevatron with a luminosity-upgrade and at the LHC.

I. INTRODUCTION

The top quark has been experimentally observed at the Fermilab Tevatron by the CDF and D0 collaborations [1] with a measured mass around 175 GeV. Because it has a mass of the order of the Fermi scale, the top quark couples quite strongly to the electroweak symmetry-breaking sector. In the Standard Model (SM), the electroweak symmetry-breaking sector consists of a complex fundamental Higgs scalar, but “triviality” [2] and “naturalness” [3] of

the scalar sector suggest that the Higgs sector may not be so simple. It is therefore plausible to assume that the mass generation mechanism is more complicated and the Higgs sector of the SM is just an effective theory, and that new physics phenomena may be manifested through effective interactions of the top quark [4].

If anomalous top-quark couplings beyond the SM exist, they will affect top-quark production and decay processes at hadron and e^+e^- colliders [5,6]. Furthermore, such couplings would certainly affect certain low-energy quantities which are measured with high precision. One such possibility is the partial width ratio $R_b = \Gamma(Z \rightarrow b\bar{b})/\Gamma(Z \rightarrow \text{Hadrons})$ measured at LEP-I, which is about 3σ higher than the Standard Model expectation [7] and could be an indication of new physics associated with the heavy top quark.

In Ref. [8], the experimental constraints on an anomalous top-quark coupling $Z\bar{t}c$ and the experimental observability of the induced rare decay mode $t \rightarrow Zc$, at the Fermilab Tevatron and the LHC at CERN, have been investigated in detail. In this paper, we examine the possible anomalous top-quark coupling $\bar{t}c\gamma$ and its implications in both low and high energy processes. In our analysis we will also allow for the possibility of a $\bar{t}cg$ coupling because it has a similar form to the $\bar{t}c\gamma$ coupling. Since the Standard Model prediction of $\Gamma(t \rightarrow c\gamma)$ is unobservably small [9], any experimental evidence for the $\bar{t}c\gamma$ coupling will be an unequivocal indication of new physics beyond the Standard Model.

This paper is organized as follows. In Section II, we examine the constraints on the anomalous $\bar{t}c\gamma(g)$ couplings from $b \rightarrow s\gamma$ and from the limit on non-standard top decays at the Tevatron. In Section III, we study the possibility of detecting the $\bar{t}c\gamma$ coupling at the Tevatron and the LHC, paying particular attention to the kinematical characteristics to extract the signal from the possible background. The cuts are adjusted to the different physics requirements at the two accelerators. Finally, in Section IV, we summarize our results.

II. CONSTRAINTS ON THE TOP-QUARK ANOMALOUS COUPLINGS

Following Ref. [4], we introduce an effective Lagrangian involving the anomalous top-quark couplings,

$$\mathcal{L}^{eff} = \mathcal{L}^{SM} + \Delta\mathcal{L}^{eff} \quad (1)$$

where \mathcal{L}^{SM} is the Standard Model Lagrangian and $\Delta\mathcal{L}^{eff}$ includes the anomalous top-quark couplings. For the purpose of this paper, we consider only the lowest dimension, CP -conserving operators which give rise to anomalous $\bar{t}c\gamma(g)$ vertices. Then

$$\Delta\mathcal{L}^{eff} = \frac{1}{\Lambda} [\kappa_\gamma e \bar{t} \sigma_{\mu\nu} c F^{\mu\nu} + \kappa_g g_s \bar{t} \sigma_{\mu\nu} \frac{\lambda^i}{2} c G^{i\mu\nu}] + h.c. , \quad (2)$$

where $F^{\mu\nu}$ ($G^{i\mu\nu}$) is the $U_{em}(1)$ ($SU_c(3)$) field strength tensor; e (g_s) is the corresponding coupling constant; and Λ is the cutoff of the effective theory, which we take to be the order of 1 TeV. The parameters κ_γ and κ_g can be interpreted as the strengths of the anomalous interactions, or, alternatively, Λ/κ is the approximate scale at which new physics in the top-quark sector occurs.

The measurement of the inclusive branching ratio for the process $b \rightarrow s\gamma$ [10] puts severe constraints on various extensions of the standard model [11]. Here we study its constraints on anomalous top-quark couplings $\bar{t}c\gamma$ and $\bar{t}cg$. Anomalous couplings of various types associated with the top quark and their constraints obtained from low-energy processes have been considered in the literature [12].

The effective Hamiltonian for $b \rightarrow s\gamma$ is given by [13,14,15],

$$H_{eff} = -\frac{4}{\sqrt{2}} G_F V_{ts}^* V_{tb} \sum_i C_i(\mu) O_i(\mu), \quad (3)$$

where i runs from 1 to 8, and μ denotes the energy scale at which H_{eff} is applied. The operators set $O_i(\mu)$ consist of six four-quark operators O_{1-6} , the electromagnetic dipole operator O_7 , and the chromo-magnetic dipole operator O_8 . At the weak scale, the only contributing operator is O_7 . However, when evolving down to the low energy scale $\mu \sim m_b$,

O_7 will mix with operator O_8 and others. Here, V_{ij} are the elements of the Cabbibo-Kobayashi-Maskawa mixing matrix.

The partial decay width for $b \rightarrow s\gamma$ is, neglecting the strange-quark mass,

$$\Gamma(b \rightarrow s\gamma) = \frac{\alpha G_F^2 m_b^5}{128\pi^4} |V_{ts}^* V_{tb} C_7(m_b)|^2. \quad (4)$$

Normalized by the inclusive semileptonic branching ratio, the $b \rightarrow s\gamma$ branching ratio can be written as

$$\frac{BR(b \rightarrow s\gamma)}{BR(b \rightarrow ce\nu)} = \frac{|V_{ts}^* V_{tb}|^2}{|V_{cb}|^2} \frac{6\alpha}{\pi g(z)} |C_7(m_b)|^2, \quad (5)$$

where $g(z) = 1 - 8z^2 + 8z^6 - z^8 - 24z^4 \ln z$, with $z = m_c/m_b$. In the standard model, the complete leading logarithmic approximation gives [15]

$$C_7(m_b) = \eta^{16/23} C_7(M_W) + \frac{8}{3} (\eta^{14/23} - \eta^{16/23}) C_8(M_W) + C_2(M_W) \sum_{i=1}^8 h_i \eta^{p^i}, \quad (6)$$

with $\eta = \alpha_s(M_W)/\alpha_s(m_b)$. The coefficients $C_2(M_W)$, h_i and p^i can be found in [15].

The anomalous top-quark couplings $\bar{t}c\gamma$ and $\bar{t}cg$ modify the coefficients of operators O_7 and O_8 . The coefficients of these operators at the electroweak scale can be written as

$$C_7(M_W) = C_7^{SM}(M_W) - \frac{1}{2} \left(\frac{V_{cs}}{V_{ts}} \right)^* \frac{m_t}{\Lambda} \ln\left(\frac{\Lambda^2}{m_t^2}\right) \kappa_\gamma, \quad (7)$$

$$C_8(M_W) = C_8^{SM}(M_W) - \frac{1}{2} \left(\frac{V_{cs}}{V_{ts}} \right)^* \frac{m_t}{\Lambda} \ln\left(\frac{\Lambda^2}{m_t^2}\right) \kappa_g, \quad (8)$$

where $C_7^{SM}(M_W)$ and $C_8^{SM}(M_W)$ are the standard model contributions.

Using $BR(b \rightarrow ce\nu) = 0.108$ and the recent CLEO measurement [10]

$$1 \times 10^{-4} < BR(b \rightarrow s\gamma) < 4.2 \times 10^{-4}, \quad (9)$$

we plot the allowed region for κ_γ and κ_g in Fig. 1, for $m_b = 5$ GeV, $m_t = 175$ GeV, $\alpha_s(M_Z) = 0.12$ and $|V_{ts}^* V_{tb}/V_{cb}|^2 = 0.95$ [15]. Throughout this paper, we take $\Lambda = 1$ TeV. In the figure there are two allowed bands: the right band corresponds to a small anomalous correction to the SM $C_7(m_b)$ coefficient which obeys the limit in Eq. (9), while the left band

corresponds to a large correction which is approximately twice the magnitude of the SM contribution but of the opposite sign, so that the magnitude of $C_7(m_b)$ is still consistent with Eq. (9).

A further restriction on κ_γ and κ_g can be obtained from the fact that $t \rightarrow cg$ and $t \rightarrow c\gamma$ decays are not the most significant top decay modes as shown by the recent CDF data [16]. A straightforward calculation of partial widths yields

$$\frac{\Gamma(t \rightarrow c\gamma)}{\Gamma(t \rightarrow bW)} = \frac{16\sqrt{2}\pi\alpha}{G_F \left(1 - \frac{M_W^2}{m_t^2}\right)^2 \left(1 + \frac{2M_W^2}{m_t^2}\right)} \left(\frac{\kappa_\gamma}{\Lambda}\right)^2, \quad (10)$$

where the masses of the c and b quarks have been ignored. For the case of $\Gamma(t \rightarrow cg)$, α is replaced by $4\alpha_s/3$ in the above equation.

The CDF data on the branching ratio of top decaying to b [16],

$$BR(t \rightarrow bW) = 0.87_{\pm 0.30}^{\pm 0.13 \pm 0.11} \quad (11)$$

places the limit

$$BR(t \rightarrow cg) < 0.45 \quad (12)$$

at the one standard deviation level, where the insignificant contribution of $t \rightarrow c\gamma$ has been ignored. This constraint gives the limit

$$|\kappa_g| < 0.9, \quad (13)$$

and is shown in Fig. 1 as the dashed lines.

One can see that $BR(b \rightarrow s\gamma)$ combined with $BR(t \rightarrow bW)$ has constrained κ_γ very strongly. The branching ratio for $t \rightarrow c\gamma$ is shown in Fig. 2(a) versus κ_γ for the maximum and minimum allowed magnitudes of κ_g . Specifically, we find that

$$\text{for } \kappa_g = 0 : |\kappa_\gamma| < 0.16 \quad \text{and} \quad BR(t \rightarrow c\gamma) < 1.3 \times 10^{-3} \quad (14)$$

$$\text{for } |\kappa_g| = 0.9 : |\kappa_\gamma| < 0.28 \quad \text{and} \quad BR(t \rightarrow c\gamma) < 2.2 \times 10^{-3}, \quad (15)$$

when accounting for the contribution of the $t \rightarrow cg$ decay to the total width. A similar constraint for the case with $\kappa_g = 0$ has been obtained in Ref. [17]. The branching ratio for $t \rightarrow cg$ is shown in Fig. 2(b) versus κ_g .

III. TOP-QUARK DECAY VIA ANOMALOUS COUPLINGS AT HADRON COLLIDERS

At the Fermilab Tevatron, the cross section for $t\bar{t}$ production is about 5 pb at $\sqrt{s} = 2$ TeV. A detailed study of top-quark decays is possible with the expected 1 fb⁻¹/yr integrated luminosity of the Main Injector, or the 10 fb⁻¹/yr anticipated at the Tevatron Upgrade [18]. Top-quark production is much greater at the LHC, with a cross section being of order 1000 pb, due to the larger center of mass energy (14 TeV) and higher integrated luminosity (100 fb⁻¹/yr). Therefore it is feasible to search for evidence of anomalous couplings such as $\bar{t}c\gamma$ at hadron colliders.

The decay $t \rightarrow c\gamma$ has already been discussed in the previous section. To obtain the signal event rate, we calculate the top-quark production via $q\bar{q}, gg \rightarrow t\bar{t}$ with the lowest order matrix elements, but normalize the total cross sections to values which include order α_s^3 corrections [19]. We thus find that the constant K factors are

$$K = 1.4 \quad \text{for Tevatron}; \quad K = 2.0 \quad \text{for LHC}.$$

For the parton distributions we use the recent parameterization MRS Set-A [20]. Due to the enormous QCD backgrounds at hadron colliders, it is very difficult, if not impossible, to search for the signal if both the top and antitop decay purely hadronically. We therefore look for events with one top-quark decay leptonically $t \rightarrow W^+b \rightarrow \ell^+\nu b$ (or $\bar{t} \rightarrow W^-\bar{b} \rightarrow \ell^-\bar{\nu}\bar{b}$), where $\ell = e, \mu$. The cross section for such events is calculated using the exact matrix elements for an on-shell W . We have ignored the spin correlations for the decaying top quarks since the top-quark production mechanisms we consider give insignificant top-quark polarization [21].

Figure 3 shows the calculated total cross section plotted versus κ_γ , for two values of κ_g , for the process $t\bar{t} \rightarrow bWc\gamma \rightarrow jj\ell^\pm\nu\gamma$, where $\ell = e, \mu$ and j represents a jet from either a b or c quark. The curves stop at the maximum allowed value of κ_γ in each case. Figure 3(a) is for the Fermilab Tevatron ($p\bar{p}$ collisions with $\sqrt{s} = 2$ TeV), and Fig. 3(b)

for the LHC (pp collisions with $\sqrt{s} = 14$ TeV). We see that for the allowed values of κ_γ , the signal cross section at the Tevatron could be as large as 4 fb, which is rather small but still might be observable at the Tevatron Upgrade. At the LHC, the maximal signal cross section is nearly 600 fb, which means that there could be a large number of events even for non-maximal couplings. We should remark that the top-quark production cross section is somewhat sensitive to the top-quark mass. For $m_t = 200$ GeV, for example, the cross section is reduced by slightly more or less than 50% at the Tevatron and the LHC, respectively.

The only irreducible backgrounds to the signal are electroweak (EW) $W^\pm\gamma$ production plus two QCD jets

$$p\bar{p} \rightarrow W^\pm\gamma jj \rightarrow \ell^\pm\nu\gamma jj. \quad (16)$$

There are also possible “fake” events

$$p\bar{p} \rightarrow W^\pm jjj \rightarrow \ell^\pm\nu\gamma jj \quad (17)$$

where one of the QCD jets fakes a photon. These backgrounds have substantial production rates. The signal is however distinctive: besides the isolated charged lepton and large missing transverse energy (E_T^{miss}) from W^\pm decay, there is a highly energetic photon, and two hard (b, c -quark) jets with which $c\gamma$ and bW both reconstruct a top (or \bar{t}). Without requiring b -tagging, our signal selection procedure is as follows: we first examine the two values of the invariant mass $M(\gamma j_1)$ and $M(\gamma j_2)$ and identify the jet which gives an $M(\gamma j)$ value closer to m_t as the c -quark jet. Naturally, the other jet will be identified as b -quark jet. Due to the missing neutrino from the W decay, the W momentum can't be reconstructed unambiguously due to the lack of knowledge of the parton c.m. frame. This is known as the two-fold ambiguity in constructing the neutrino momentum along the beam direction [22]. Taking the W mass as an input and for massless leptons, using the measured charged lepton momentum (p^ℓ) and the *transverse* momentum (with respect to the beam direction) of the neutrino (p_T^ν), the two solutions for the *longitudinal* momentum of the neutrino can be expressed by

$$p_L^\nu = \frac{1}{2(p_T^\ell)^2} \left\{ p_L^\ell (M_W^2 + 2\mathbf{p}_T^\ell \cdot \mathbf{p}_T^\nu) \pm p^\ell \left[(M_W^2 + 2\mathbf{p}_T^\ell \cdot \mathbf{p}_T^\nu)^2 - 4(p_T^\ell)^2 (p_T^\nu)^2 \right]^{1/2} \right\}. \quad (18)$$

There are therefore two solutions for p_W , correspondingly. We again take the one that gives an $M(bW)$ value closer to m_t . With this procedure, both top-quark momenta are experimentally identifiable.

To make the calculation more realistic, we simulate the detector effects by assuming a Gaussian energy smearing for the electromagnetic and hadronic calorimetry as follows:

$$\begin{aligned} \Delta E/E &= 30\%/\sqrt{E} \oplus 1\%, & \text{for lepton and photon} \\ &= 80\%/\sqrt{E} \oplus 5\%, & \text{for jets,} \end{aligned} \quad (19)$$

where the \oplus indicates that the E -dependent and E -independent errors are to be added in quadrature, and E is to be measured in GeV.

A. Tevatron

To quantify the experimental sensitivity to the anomalous couplings, we first impose acceptance cuts on the transverse momentum (p_T), pseudo-rapidity (η), and the separation in the azimuthal angle-pseudo rapidity plane (ΔR) for the charged lepton and photon from the jets. We choose the following ‘‘basic’’ acceptance cuts:

$$\begin{aligned} p_T^\ell > 15 \text{ GeV}, & \quad p_T^j > 20 \text{ GeV}, & \quad p_T^\gamma > 30 \text{ GeV}, & \quad E_T^{miss} > 20 \text{ GeV}, \\ |\eta^\ell|, |\eta^\gamma|, |\eta^j| < 2.5, & \quad \Delta R_{\ell j}, \Delta R_{jj}, \Delta R_{\gamma j} > 0.4. \end{aligned} \quad (20)$$

The high transverse momentum thresholds for the jets and the photon are motivated by the hard p_T spectrum from the heavy top decay. With these basic cuts, the signal rate in Fig. 3(a) is reduced by about 40% (with a maximal value of about 2.7 fb), while the EW irreducible background of Eq. (16) is about 30 fb, and the QCD process for $\ell^\pm \nu jjj$ production in Eq. (17) is about 3000 fb. It has been shown that the fake rate for a jet to a photon ($j \rightarrow \gamma$) at the Tevatron experiments [23] can be controlled down to a level of 10^{-4}

for $p_T^\gamma > 25$ GeV, making it insignificant. Therefore, the EW background dominates and we will consequently concentrate on that.

Figure 4(a) shows the reconstructed distributions for the top-antitop invariant mass. Obviously, $M(t\bar{t})$ for the signal has a kinematical lower limit ($2m_t$ if no energy smearing is applied); while the lower limit is significantly smaller for the background, near the $W\gamma jj$ threshold. If we only accept events with

$$M(t\bar{t}) > 2m_t = 350 \text{ GeV}, \quad (21)$$

we expect to improve the signal-to-background ratio (S/B). Also, due to the nature of top-quark two-body decay, the final state jets and the photon have transverse momenta typically the order of $\frac{1}{2}m_t \simeq 80$ GeV, while all the jets and photon in the background events tend to be soft. To further discriminate the signal from the background, we define two scalar sums of the transverse momenta:

$$p_T(cb) \equiv |\vec{p}_T^c| + |\vec{p}_T^b|, \quad p_T(cb\gamma) \equiv p_T(cb) + |\vec{p}_T^\gamma|.$$

Figure 4(b) shows the distributions for these variables. We see indeed that the signal spectra are much harder at the low end. On the other hand, they are limited by the physical scale $2m_t$ for the signal at the high end, while they extend further for the background. With these in mind, our choices of the cuts are

$$100 < p_T(cb) < 300 \text{ GeV}, \quad 150 < p_T(cb\gamma) < 450 \text{ GeV}. \quad (22)$$

With the additional cuts of Eqs. (21) and (22), the EW background is reduced to about 10 fb, while the signal may be as large as 2.4 fb.

In Fig. 5 we show the reconstructed top-quark mass distributions $M(c\gamma)$ and $M(bW)$, after making the additional cuts in Eqs. (21) and (22). We see from Fig. 5(a) that, despite the improvement in S/B , the continuum background is still above the $M(c\gamma)$ signal peak at m_t . Further improvement can be made if we only study the events with

$$|M(c\gamma) - m_t| < 20 \text{ GeV}. \quad (23)$$

The short-dashed histogram in Fig. 5(b) shows how the background in the $M(bW)$ distribution is reduced by the cut Eq. (23). We find that the signal peak is nearly unaffected by this cut and is now above the background, so that statistically significant effects may be observed near m_t in the $M(bW)$ spectrum. If we examine the events in the mass range

$$|M(bW) - m_t| < 30 \text{ GeV}, \quad (24)$$

the signal observability should be nearly optimized. After the cut in Eq. (24) we are left with a maximal signal of 2.0 fb and an EW background 1.8 fb.

B. LHC

At the LHC energy, due to the more complicated hadronic backgrounds, we need to increase the transverse momentum thresholds, especially for jets, direct photons and missing E_T . We adopt the “basic” acceptance cuts as

$$p_T^\ell > 20 \text{ GeV}, \quad p_T^j > 35 \text{ GeV}, \quad p_T^\gamma > 40 \text{ GeV}, \quad E_T^{miss} > 30 \text{ GeV}, \\ |\eta^\ell|, |\eta^\gamma|, |\eta^j| < 3, \quad \Delta R_{\ell j}, \Delta R_{jj}, \Delta R_{\gamma j} > 0.4. \quad (25)$$

The signal rates given in Fig. 3(b) are reduced by about 60% with the cuts of Eq. (25) (with a maximal value of about 0.22 pb), while the EW background is about 0.5 pb, and the “faked” QCD background is about 70 pb. Assuming that we can effectively reject the QCD background by photon identification to a level of 10^{-3} for $j \rightarrow \gamma$ [24], then the dominant background is again the electroweak process. We see that after the basic cuts of Eq. (25) the S/B ratio is much closer to unity than in the Tevatron case.

Similar to the Tevatron study, we have constructed distributions for the top-antitop invariant mass and scalar sums of transverse momenta (see Fig. 6). We see that further background suppression can be achieved, without much loss of signal, by the cuts of Eqs. (21) and (22). The signal integrated cross section after these cuts may be as large as 200 fb, while the EW background rate is about 300 fb.

As at the Tevatron, reconstructed top-quark mass distributions are also crucial to non-ambiguously identify the signal. Figure 7 shows the top-quark mass distributions reconstructed from the $c\gamma$ and bW final states after making the cuts in Eqs. (21) and (22). Once the final cuts in Eqs. (23) and (24) are made, the signal integrated cross section has a maximal value of 175 fb and the EW background is 33 fb. We see that the S/B ratio is significantly better than at the Tevatron, primarily due to the huge enhancement for the $t\bar{t}$ production at higher c.m. energies.

C. b -tagging Effects

The CDF collaboration were able to achieve about 50% b -tagging efficiency [25] and one hopes to reach about the same efficiency for the LHC experiments [24]. The impurity from the light quarks/gluons is assumed to be 1%. We therefore can naively expect to further suppress the backgrounds by a factor of $1\% \times n_j$ (where n_j is the number of jets) at a cost of signal reduction of 50%.

One has to be cautious in making this statement since there is direct production of $b\bar{b}$ among the other light quark/gluon jets in the background events. We have explicitly calculated the $W\gamma b\bar{b}$ production rate and found the cross section is about 0.12 fb at the Tevatron and 1.1 fb at the LHC with the basic cuts plus Eqs. (21) and (22). This implies that the misidentified b from light quarks/gluons is indeed the major background source. Consequently, we will not carry out the calculation for the $b\bar{b}$ fraction in $Wjjj$ events, since this channel is always smaller to begin with.

Table I lists the signal rate (for $\kappa_g = 0, \kappa_\gamma = 0.16$), EW and QCD backgrounds at the Tevatron and the LHC. Comparison is made for the results with only cuts of Eq. (20) for Tevatron or Eq. (25) for LHC and Eqs. (21) and (22), and those plus b -tagging. We indeed obtain significant improvement for the signal/background ratios, although the signal rate at the Tevatron is very limited.

IV. DISCUSSIONS AND SUMMARY

To estimate the sensitivity to the anomalous couplings for a given accumulated luminosity, we first establish the approximate cross section formula for the $t \rightarrow c\gamma$ case in terms of the anomalous couplings:

$$\sigma = \frac{\kappa_\gamma^2}{(1 + 1.04\kappa_g^2)^2} \sigma(\kappa_\gamma = 1, \kappa_g = 0) \quad (26)$$

where $\sigma(\kappa_\gamma = 1, \kappa_g = 0)$ is calculated for the appropriate set of cuts, and the couplings are subject to the constraints in Fig. 1. The cross section $\sigma(\kappa_\gamma = 1, \kappa_g = 0)$ is 80 fb and 6.8 pb at the Tevatron and LHC, respectively, after the full set of cuts is made. We start with Poisson statistics since the signal rate is often small, especially at the Tevatron energy. Figure 8 presents the anomalous coupling κ_γ versus the luminosity needed to probe κ_γ at 95% Confidence Level (CL).¹ The solid curves presented in each panel are for $\kappa_g = 0$ and the dashed for $|\kappa_g| = 0.9$. The upper curves for each case are those with kinematical cuts only, while the lower ones are that including b -tagging improvement. We see that at the Tevatron energy, minimal luminosity of about 5 fb^{-1} is needed in order to probe κ_γ near the current low energy constraints at 95% CL. At the LHC with 100 fb^{-1} , one expects to improve the sensitivity to κ_γ by more than one order of magnitude. For instance, for $\kappa_g = 0$ and with b -tagging, the sensitivity at the Tevatron reaches

$$\begin{aligned} \text{for } 5 \text{ fb}^{-1} : |\kappa_\gamma| &\sim 0.16 \quad \text{and} \quad BR(t \rightarrow c\gamma) \sim 1.3 \times 10^{-3} \\ 10 \text{ fb}^{-1} : |\kappa_\gamma| &\sim 0.12 \quad \text{and} \quad BR(t \rightarrow c\gamma) \sim 7 \times 10^{-4} \\ 30 \text{ fb}^{-1} : |\kappa_\gamma| &\sim 0.08 \quad \text{and} \quad BR(t \rightarrow c\gamma) \sim 3 \times 10^{-4}, \end{aligned} \quad (27)$$

and at the LHC

¹In our approach, a 95% CL in Poisson statistics roughly corresponds to $S/\sqrt{S+B} = 3$ in Gaussian statistics when the number of events is large.

$$\begin{aligned}
\text{for } 10 \text{ fb}^{-1} : |\kappa_\gamma| \sim 0.02 \quad \text{and} \quad BR(t \rightarrow c\gamma) \sim 2 \times 10^{-5} \\
100 \text{ fb}^{-1} : |\kappa_\gamma| \sim 0.01 \quad \text{and} \quad BR(t \rightarrow c\gamma) \sim 5 \times 10^{-6},
\end{aligned}
\tag{28}$$

Alternatively, setting $\kappa_\gamma = 1$ and letting Λ vary (see Eq. (2)), we can view this as a probe of the scale of new physics up to $\Lambda/\kappa_\gamma \sim 10$ TeV at the Tevatron and about 100 TeV at the LHC.

If $\kappa_g \neq 0$, there of course is also the possibility of $t \rightarrow cg$ decay, which is only mildly constrained by current Tevatron data. Although the hadronic nature of the decay might make the detection of this mode difficult, the jets resulting from this decay will have large transverse momentum, and may allow one to distinguish the signal from the background. There is also the possibility of single top production in association with a charm quark [26]. The phenomenology of the $\bar{t}cg$ coupling at hadron colliders is currently under study [27].

V. ACKNOWLEDGMENTS

We would like to thank Liangxin Li for collaboration in the calculation of the $b \rightarrow s\gamma$ limits during an early stage of this work. We thank Roberto Peccei for discussions. BLY would like to thank Hai-Yang Cheng and Shih-Chang Lee for warm hospitality extended to him during his sabbatical leave at the Institute of physics, Academia Sinica, Taipei, when part of the work was performed. He would also like to thank the National Science Council for financial support. XZ thanks G. Buchalla for discussions. This work was supported in part by the U.S. Department of Energy under Contracts DE-FG03-91ER40674 (T. Han) and DE-FG02-94ER40817 (K. Whisnant, B.-L. Young and X. Zhang).

TABLES

TABLE I. Cross sections in units of fb for the $t\bar{t} \rightarrow \ell^\pm \nu bc\gamma$ signal ($\kappa_g = 0, \kappa_\gamma = 0.16$), and EW and QCD backgrounds at the Tevatron and the LHC. Comparison is made for the results with only cuts Eqs. (20 or 25) and (21-22) and those plus b -tagging. 50% tagging efficiency and 1% impurity are assumed [25].

(a). Tevatron	signal $t\bar{t} \rightarrow \ell^\pm \nu bc\gamma$	$W\gamma jj \rightarrow \ell^\pm \nu \gamma jj$	$Wjjj \rightarrow \ell^\pm \nu \gamma jj$
cuts only	2.4	10	0.66
plus b -tag	1.2	0.3	0.01
(b). LHC	signal $t\bar{t} \rightarrow \ell^\pm \nu bc\gamma$	$W\gamma jj \rightarrow \ell^\pm \nu \gamma jj$	$Wjjj \rightarrow \ell^\pm \nu \gamma jj$
cuts only	200	300	45
plus b -tag	100	7	1

REFERENCES

- [1] F. Abe et al. (CDF Collaboration), Phys. Rev. Lett. **74**, 2626 (1995); S. Abachi et al. (D0 Collaboration), Phys. Rev. Lett. **74**, 2632 (1995).
- [2] For a recent review, see, *e. g.*, H. Neuberger, in *Proceedings of the XXVI International Conference on High Energy Physics*, Dallas, Texas, 1992, edited by J. Sanford, AIP Conf. Proc. No. 272 (AIP, New York, 1992), Vol. II, p. 1360.
- [3] G. 't Hooft, in *Recent Developments in Gauge Theories*, Proceedings of the Cargese Summer Institute, Cargese, France, 1979, edited by G. 't Hooft et al., NATO Advanced Study Institute Series B; Physics Vol. 59 (Plenum, New York, 1980).
- [4] R. D. Peccei and X. Zhang, Nucl. Phys. **B337**, 269 (1990).
- [5] See, *e. g.*, D. O. Carlson, E. Malkawi and C.-P. Yuan, Phys. Lett. **B337**, 145 (1994); and references therein.
- [6] See, *e. g.*, D. Atwood, A. Kagan and T. Rizzo, Phys. Rev. **D52**, 6264 (1995); and references therein.
- [7] P. B. Renton, talk presented at *the 17th International Symposium on Lepton-Photon Interactions*, Beijing, August 1995.
- [8] T. Han, R.D. Peccei and X. Zhang, Nucl. Phys. **B454**, 527 (1995).
- [9] B. Grzadkowski, J.F. Gunion and P. Krawczyk, Phys. Lett. **B268**, 106 (1991); G. Eilam, J.L. Hewett and A. Soni, Phys. Rev. **D44**, 1473 (1991); M. Luke and M.J. Savage, Phys. Lett. **B307**, 387 (1993); G. Couture, C. Hamzaoui and H. König, Phys. Rev. **D52**, 1713 (1995).
- [10] M. Alam *et al.*, CLEO collaboration, Phys. Rev. Lett. **74**, 2885 (1995).
- [11] J.L. Hewett, SLAC-PUB-6521 (May 1994), in *SLAC Summer Institute 1993*.

- [12] J.L. Hewett and T. Rizzo, Phys. Rev. **D49**, 319 (1994); K. Fujikawa and A. Yamada, Phys. Rev. **D49**, 5890 (1994).
- [13] B. Grinstein, R. Springer and M. Wise, Nucl. Phys. **B339**, 269 (1990).
- [14] M. Ciuchini, E. Franco, G. Martinelli, L. Reina and L. Silvestrini, Phys. Lett. **B316** 127 (1993); M. Ciuchini, E. Franco, L.Reina and L. Silvestrini, Nucl. Phys. **B421**, 41 (1994).
- [15] A.J. Buras, M. Misiak, M. Münz and S. Pokorski, Nucl. Phys. **B424**, 374 (1994).
- [16] J. Incandela (CDF Collaboration), FERMILAB-CONF-95-237-E (July 1995). In our calculation we use the branching ratio $BR(t \rightarrow bW) = 0.87_{\pm 0.32}^{+0.13}$, where the two sets of errors are combined in quadrature.
- [17] R. Martinez, M.A. Perez and J.J. Toscano, Phys. Lett. **B340**, 91 (1994).
- [18] S. Holmes, G. Dugan, and S. Peggs, in *Proceedings of the 1990 Summer Study on High Energy Physics: Research Directions for the Decade*, Snowmass, CO, ed. E.L. Berger, p. 674.
- [19] R.K. Ellis, Phys. Lett. **B259**, 492 (1991); P. Nason, S. Dawson and R.K. Ellis, Nucl. Phys. **B303**, 607 (1988); W. Beenakker et al., Nucl. Phys. **B351**, 507 (1991).
- [20] A.D. Martin, R.G. Roberts and W.J. Stirling, Phys. Rev. **D50**, 6734 (1994).
- [21] V. Barger, J. Ohnemus and R. Phillips, Int. J. Mod. Phys. **A4**, 617 (1989).
- [22] J. Stroughair and C. Bilchak, Z. Phys. **C26**, 415 (1984); J. Gunion, Z. Kunszt, and M. Soldate, Phys. Lett. **B163**, 389 (1985); J. Gunion and M. Soldate, Phys. Rev. **D34**, 826 (1986); W. J. Stirling *et al.*, Phys. Lett. **B163**, 261 (1985); J. Cortes, K. Hagiwara, and F. Herzog, Nucl. Phys. **B278**, 26 (1986).
- [23] See, *e. g.*, H. Aihara, in proceedings of *International Symposium on Vector Boson Self-Interactions*, ed. U. Baur *et al.*, Los Anglese, CA, Feb. 1995, p. 72.

- [24] CMS Collaboration, Technical Proposal, CERN/LHCC/94-38; ATLAS Collaboration, Technical Proposal, CERN/LHCC/94-43.
- [25] F. Abe et al., (CDF Collaboration), Phys. Rev. **D52**, 2605 (1995).
- [26] E. Malkawi and T. Tait, Michigan State preprint MSUHEP-51116, November 1995.
- [27] T. Han, M. Hosch, K. Whisnant, B.-L. Young and X. Zhang, manuscript in preparation.

FIGURE CAPTIONS

FIG. 1 Constraints on anomalous couplings κ_g and κ_γ from $BR(b \rightarrow s\gamma)$ (the two diagonal bands in solid lines) and $BR(t \rightarrow bW)$ (dashed horizontal lines). $\Lambda = 1$ TeV is assumed throughout the paper.

FIG. 2 (a) Branching ratios for (a) $t \rightarrow c\gamma$ versus $|\kappa_\gamma|$ for $|\kappa_g| = 0$ (solid line) and $|\kappa_g| = 0.9$ (dashed line), and (b) $t \rightarrow cg$ versus $|\kappa_g|$. The curves stop at the maximum allowed value of the abscissa in each case.

FIG. 3 Production cross section for $t\bar{t} \rightarrow bWc\gamma \rightarrow b\ell\nu c\gamma$ at (a) the Tevatron ($p\bar{p}$) with $\sqrt{s} = 2$ TeV, and (b) the LHC (pp) with $\sqrt{s} = 14$ TeV. The top-quark mass $m_t = 175$ GeV is used throughout the paper. The cross sections are plotted versus $|\kappa_\gamma|$ for $|\kappa_g| = 0$ (solid line) and $|\kappa_g| = 0.9$ (dashed line). The curves stop at the maximum allowed value of $|\kappa_\gamma|$ in each case.

FIG. 4 (a) Top-antitop invariant mass distributions for the signal $t\bar{t} \rightarrow Wbc\gamma$ (solid histogram) and background $p\bar{p} \rightarrow Wjj\gamma$ (dashed histogram) at the Tevatron with $\sqrt{s} = 2$ TeV, assuming the basic acceptance cuts defined in Eq. (20) in the text. (b) Distributions for the transverse momenta scalar sums $p_T(bc)$ and $p_T(bc\gamma)$ for the signal (solid histograms) and background (dashed histograms). The signal histograms assume the maximal allowed value of κ_γ with $\kappa_g = 0$.

FIG. 5 Reconstructed top-quark mass distributions for (a) $M(c\gamma)$ and (b) $M(bW)$ at the Tevatron with $\sqrt{s} = 2$ TeV. In (a), the solid histogram shows the signal $t\bar{t} \rightarrow Wbc\gamma$ and the short dashed histogram shows the background $p\bar{p} \rightarrow Wjj\gamma$ after applying basic cuts and cuts on the top-antitop invariant mass and the transverse momenta scalar sums $p_T(bc)$ and $p_T(bc\gamma)$, while in (b) the same curves are used to show the signal and background after making the further cut on $M(c\gamma)$. The long dashed histogram in (b) shows the $M(bW)$ distribution of the background before $M(c\gamma)$ cut is made (the effect of the $M(c\gamma)$ cut on

the signal is minimal). The signal histograms assume the maximal allowed value of κ_γ with $\kappa_g = 0$.

FIG. 6 (a) Top-antitop invariant mass distributions for the signal $t\bar{t} \rightarrow Wbc\gamma$ (solid histogram) and background $p\bar{p} \rightarrow Wjj\gamma$ (dashed histogram) at the LHC with $\sqrt{s} = 14$ TeV, assuming the basic acceptance cuts defined in Eq. (25) in the text. (b) Distributions for the transverse momenta scalar sums $p_T(bc)$ and $p_T(bc\gamma)$ for the signal (solid histograms) and background (dashed histograms). The signal histograms assume the maximal allowed value of κ_γ with $\kappa_g = 0$.

FIG. 7 Reconstructed top-quark mass distributions for (a) $M(c\gamma)$ and (b) $M(bW)$ at the LHC with $\sqrt{s} = 14$ TeV. In (a), the solid histogram shows the signal $t\bar{t} \rightarrow Wbc\gamma$ and the short dashed histogram shows the background $p\bar{p} \rightarrow Wjj\gamma$ after applying basic cuts and cuts on the top-antitop invariant mass and the transverse momenta scalar sums $p_T(bc)$ and $p_T(bc\gamma)$, while in (b) the same curves are used to show the signal and background after making the further cut on $M(c\gamma)$. The long dashed histogram in (b) shows the $M(bW)$ distribution of the background before $M(c\gamma)$ cut is made (the effect of the $M(c\gamma)$ cut on the signal is minimal). The signal histograms assume the maximal allowed value of κ_γ with $\kappa_g = 0$.

FIG. 8 95% CL sensitivity to κ_γ vs. integrated luminosity for (a) the Tevatron with $\sqrt{s} = 2$ TeV and (b) the LHC with $\sqrt{s} = 14$ TeV. We consider the limits for $\kappa_g = 0$ (solid lines) and $|\kappa_g| = 0.9$ (dashed lines). The upper curves in each case correspond to the limit obtained when comparing the signal and background after making all the cuts, while the lower curves correspond to the limits obtained when using b -tagging with the cuts in Eqs. (20 or 25) and (21-22). The curves cut off at the maximal allowed value of κ_γ in each case.

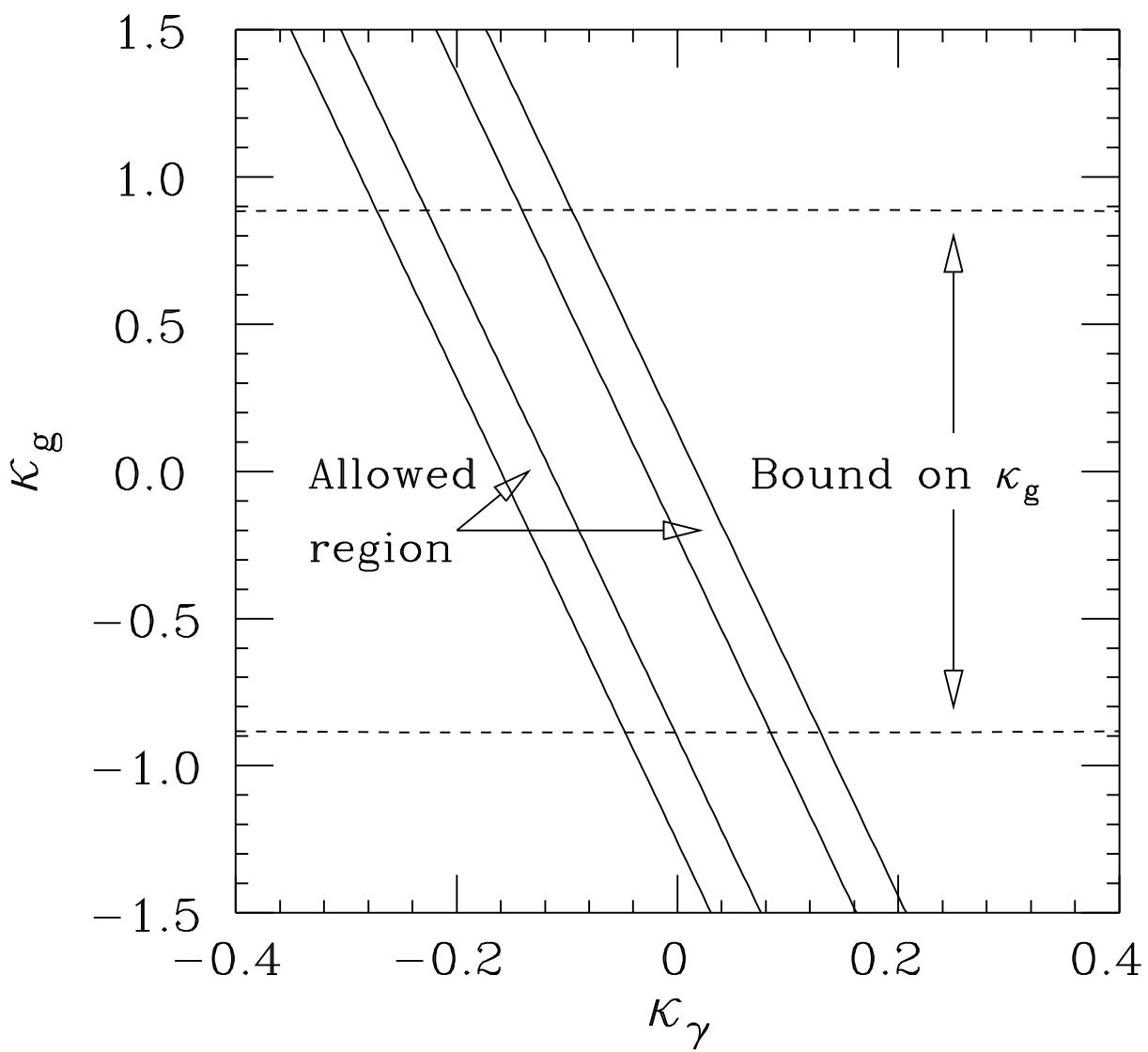


Figure 1

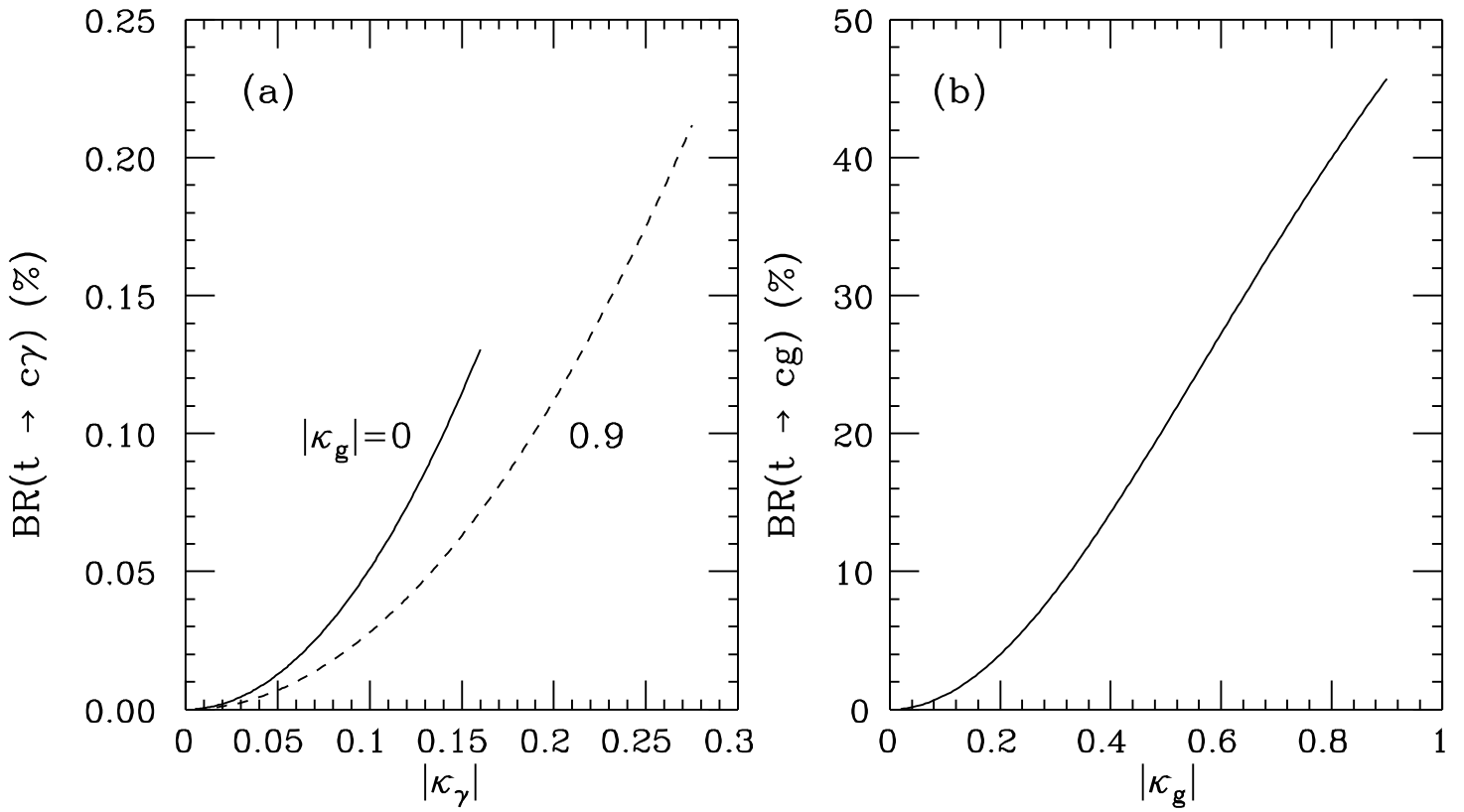


Figure 2

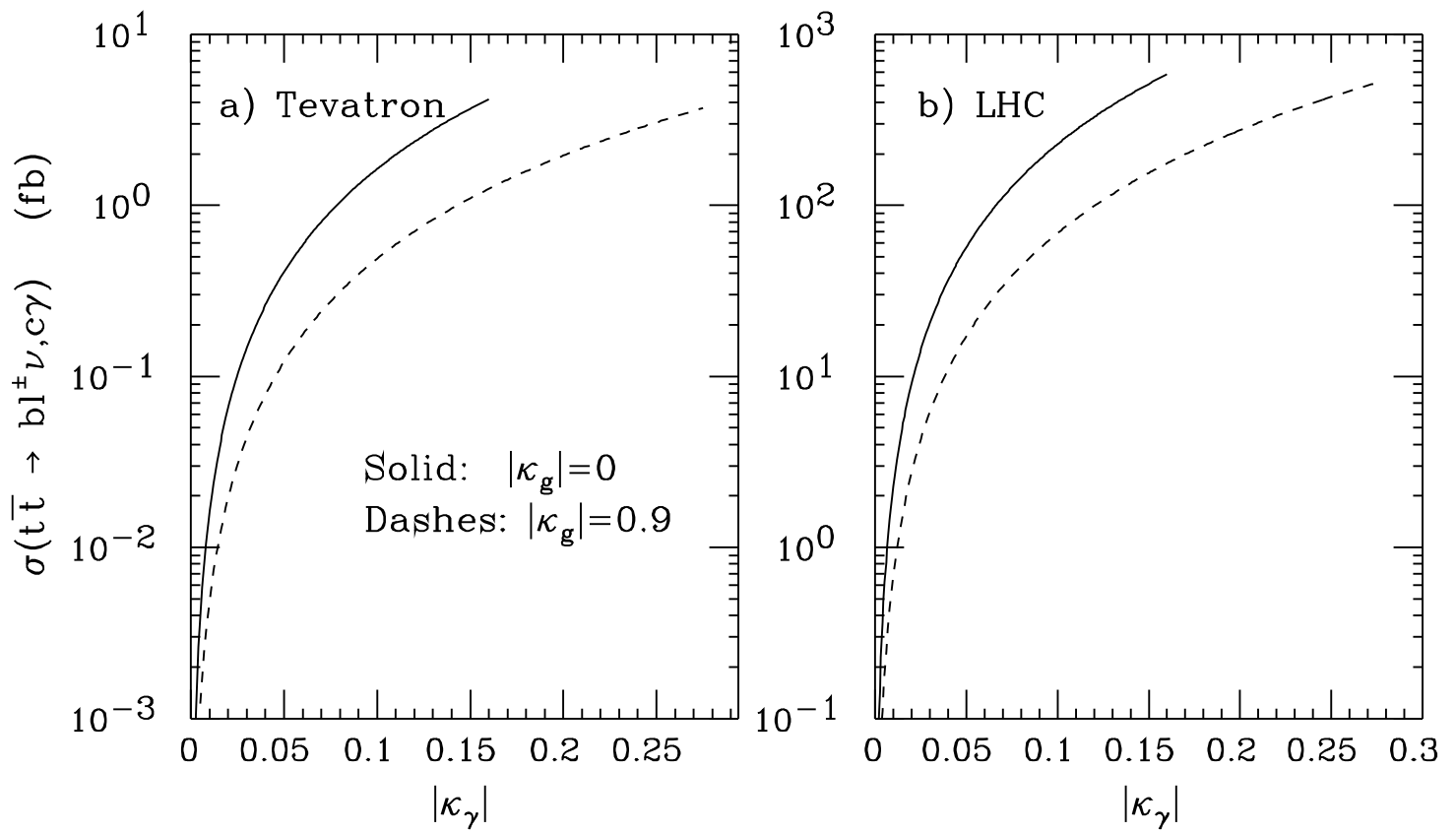


Figure 3

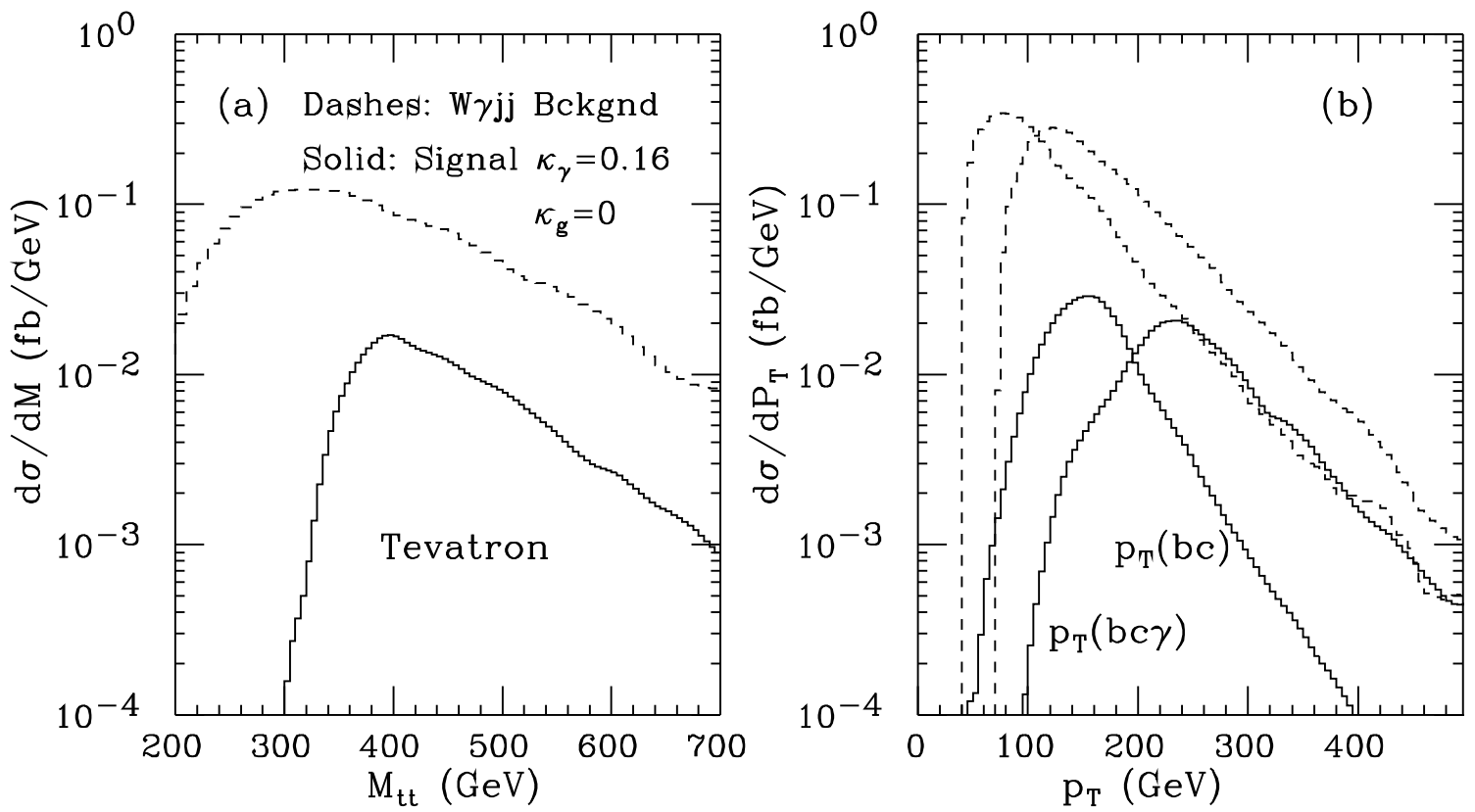


Figure 4

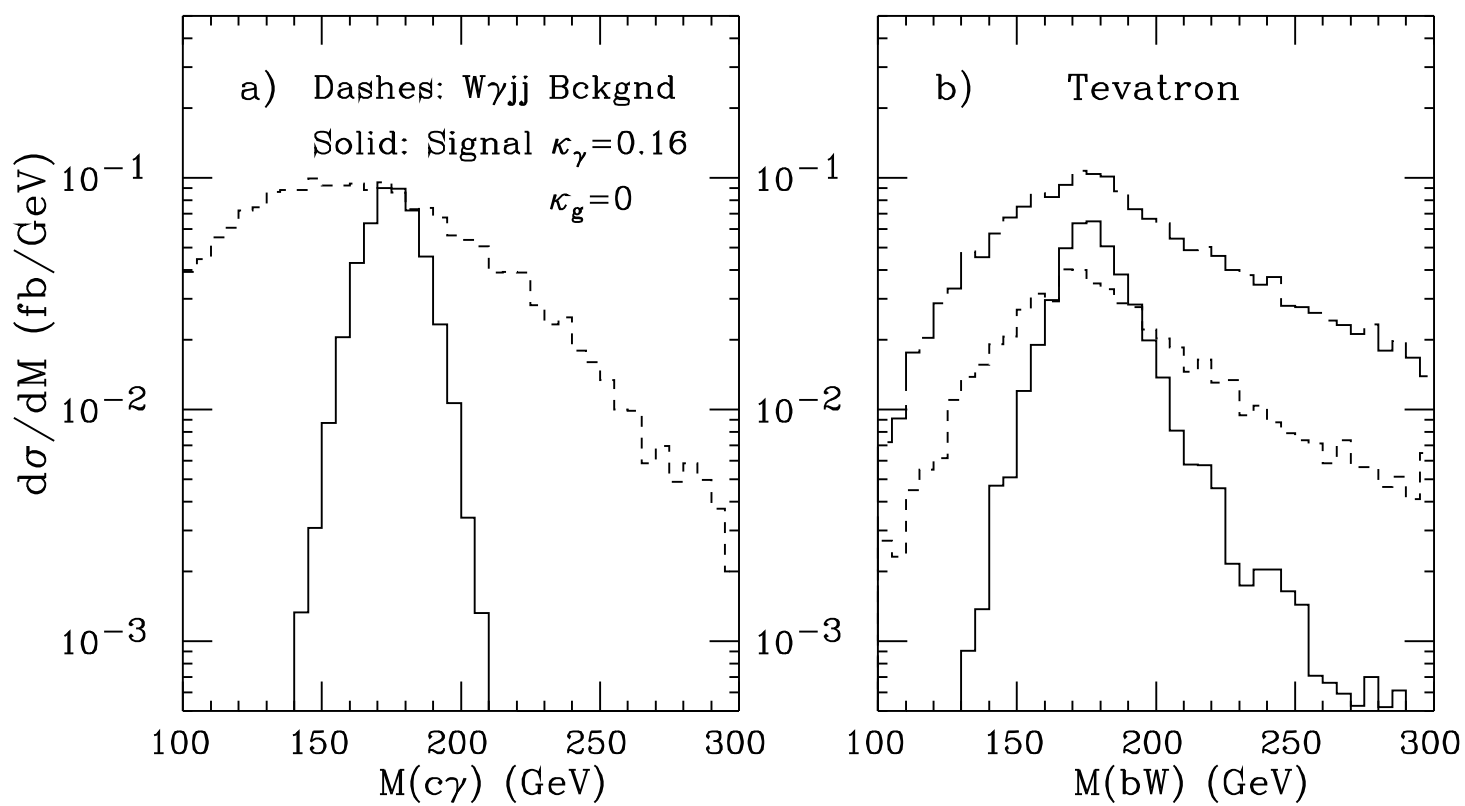


Figure 5

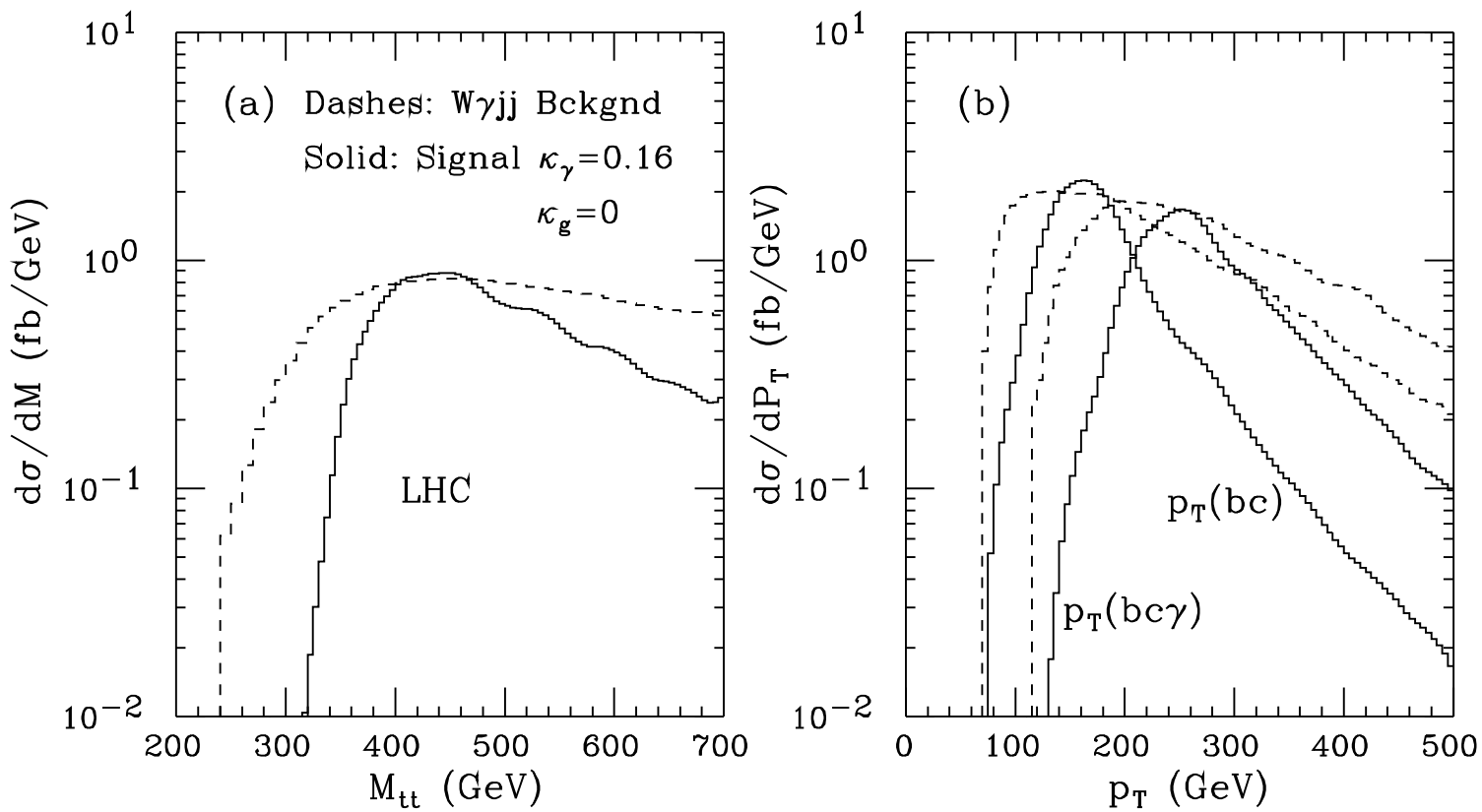


Figure 6

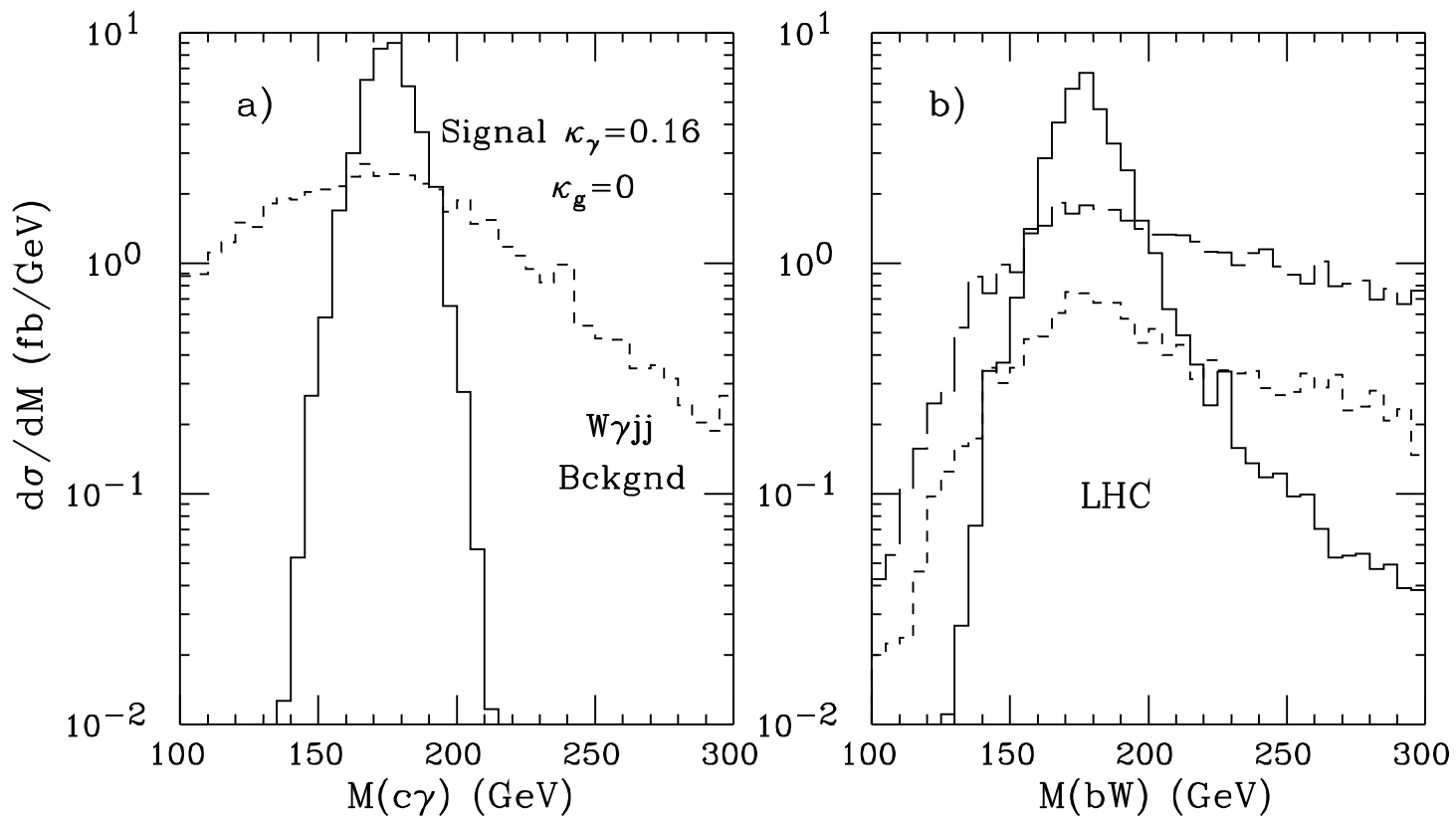


Figure 7

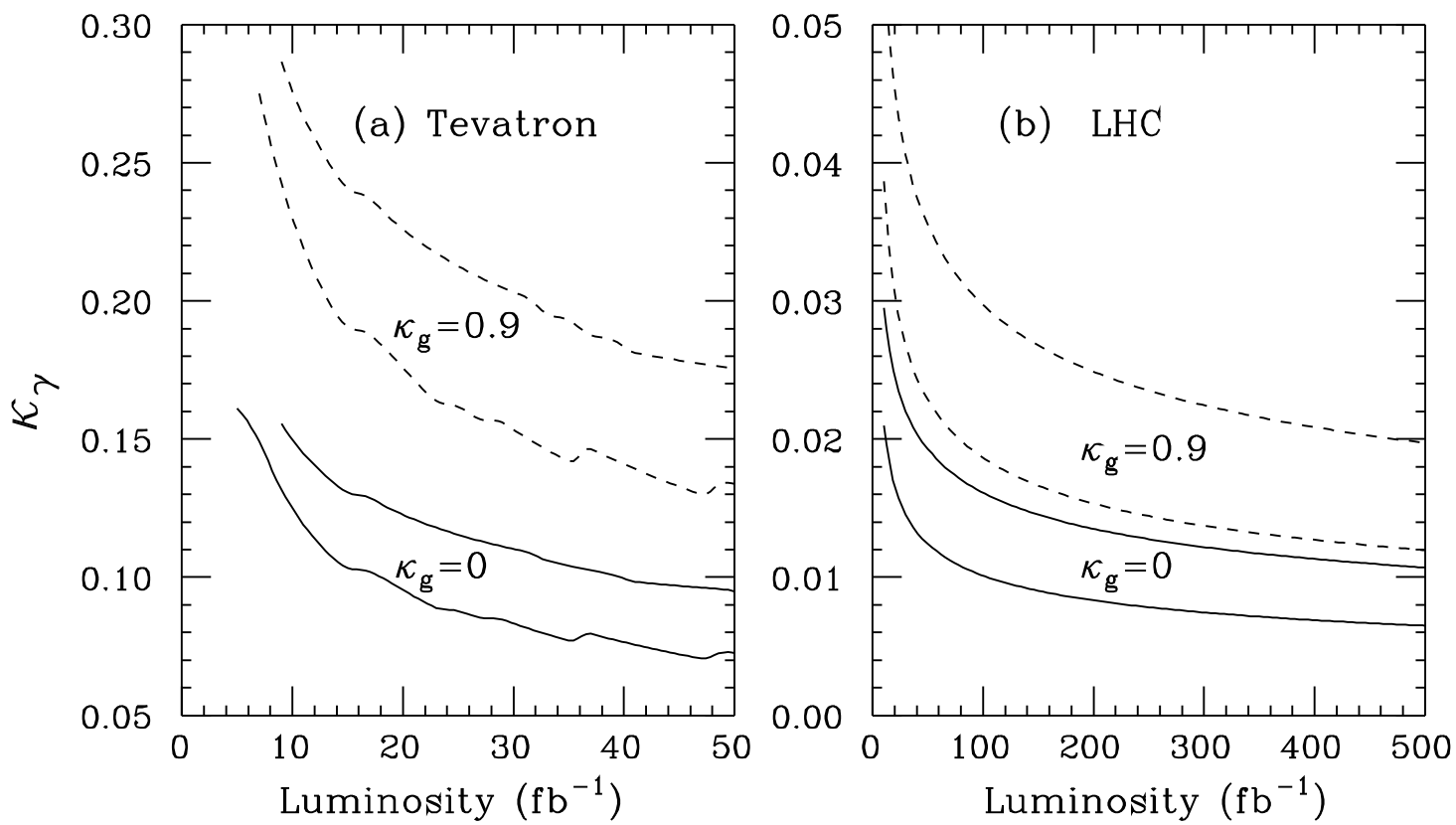


Figure 8